EDGE ARTICLE

Check for updates

All publication charges for this article have been paid for by the Royal Society of Chemistry

Mechanical insulation of aza-Pechmann dyes within [2]rotaxanes†

Guillermo Cutillas-Font, [ID] [a] Aurelia Pastor, [ID] *[a] Mateo Alajarin, [ID] [a] Alberto Martinez-Cuezva, [ID] [a] Marta Marin-Luna, [ID] [a] Belen Batanero [ID] [b] and Jose Berna [ID] *[a]

Aza-Pechmann derivatives have emerged as interesting building blocks for the preparation of organic electronic devices. The development of methodologies aimed to enhance their chemical stability and modulate their physical and chemical properties constitutes an interesting goal. Here we report the synthesis of mechanically interlocked aza-Pechmann dyes with benzylic amide macrocycles, along with the study of how the mechanical bond impacts their stability, photophysical and redox properties. Rotaxanes composed of Pechmann dilactams as threads exhibit one of the highest energy barriers for macrocyclic ring rotation, highlighting the strength of the attractive interactions ring-thread within the interlocked structure. Their enhanced thermal stability, compared to the non-interlocked counterparts, evidences the protective role of the macrocycle. Computational and electrochemical analyses indicate that the benzylic amide macrocycle improves the stability of the HOMO and LUMO orbitals of the interlocked dyes. Finally, spectroscopic and electrochemical data reveal that the macrocycle subtly modulates the optoelectronic and redox behaviour of the Pechmann dilactams.
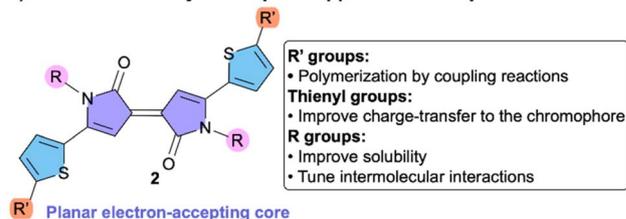
Introduction

(*E*)-3,3′-Bifuranyliden-2,2′-diones **1** (Ar = Ph, Fig. 1a), belonging to a family of compounds known as Pechmann dyes,[1,2] have remained largely unexplored due to their extremely low solubility.[3–7] (*E*)-3,3′-Bipyrrolylidene-2,2′(1*H*,1′*H*)-diones **2**, also known as Pechmann dilactams or aza-Pechmann dyes, derive from **1** by two-fold amidation.[8] Aza-Pechmann derivatives have shown good properties as colorants and dyes on several types of textiles.[1,9,10] Furthermore, Pechmann dilactams flanked by two thiophene-derived moieties have emerged in the last decade as interesting building blocks for the preparation of organic electronic devices due to: (i) their planar, conjugated core highly prone to donor–acceptor and π–π stacking interactions; (ii) the
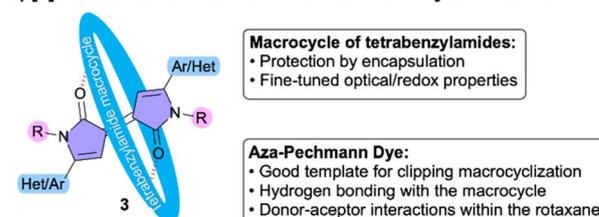
[a]Department of Organic Chemistry, Faculty of Chemistry, University of Murcia, Regional Campus of International Excellence, Campus Mare Nostrum, 30100 Murcia, Spain. E-mail: aureliap@um.es; ppberna@um.es

[b]Department of Organic Chemistry and Inorganic Chemistry, University of Alcala, Institute of Chemical Research AndrésM. del Rio, 28805 Alcalá de Henares, Madrid, Spain

† Electronic supplementary information (ESI) available: Synthesis and experimental data of compounds **2** and **3**. ESI-HRMS spectra of all new compounds. Crystal data and structure refinement for **3b** and **3c**. Determination of the constant rates and activation parameters for the pirouetting of the macrocycle in **3a** and **3c**. Thermolysis study of **2b**, **2c** and **3b**, **3c**. TGA experiments of **2b**, **2c** and **3a–c**. UV-vis spectra of **2** and **3**. Computational study and electrochemical analysis of **2** and **3**. NMR spectra of all new synthesized compounds. CCDC 2335405 (for **3b**) and 2335404 (for **3c**). For ESI and crystallographic data in CIF or other electronic format see DOI: https://doi.org/10.1039/d4sc03657c

Fig. 1 (a) Skeleton of Pechmann dyes (**1**) and Pechmann dilactams (**2**); (b) framework of a Pechmann dilactam **2** which has found applications in optoelectronics and, (c) potential benefits from encapsulation of aza-Pechmann dyes within [2]rotaxanes **3**.

alkyl chains at the nitrogen atoms, increasing its solubility and guiding the packing in the solid state, and (iii) the appropriate substitution at the thienyl groups assisting the formation of polymers by coupling reactions (Fig. 1b).[11–14] Liu, Zhang and coworkers revealed the high potential of Pechmann dilactams as building blocks to prepare OFETs with p-type,[15,16] ambipolar semiconducting properties[17–20] or active layers for organic photovoltaic devices.[21] Unfortunately, drawbacks for the use of Pechmann dilactams **2** in organic electronics are: (a) their tendency to aggregation, potentially altering their photophysical properties; and even more importantly, (b) the isomerization of 5,5-*exo*-fused Pechmann dilactams **2** to their corresponding 6,6-*endo*-fused counterparts.[8,11,13]

Accordingly, the development of methodologies aimed to enhance the chemical stability and modulate the physical and chemical properties of aza-Pechmann dyes constitutes an intriguing objective not yet addressed. Rotaxane formation provides a unique strategy to improve the properties of chromophores without altering their covalent structure (Fig. 1c). Unlike inclusion complexes, rotaxane-encapsulated dyes have the significant advantage of not being able to dissociate due to their bulky stoppers.[22,23] On one hand, the macrocycle provides steric protection increasing the chemical and thermal stability,[24,25] while also preventing aggregation that can interfere with their optoelectronic properties. On the other hand, it allows the environment around the chromophore to be precisely controlled, enabling the fine-tuning of photochemical and redox properties.[26–28] Smith and coworkers designed a [2]rotaxane with fluorescent squaraine dyes as threads.[29–31] The corresponding rotaxanes, with enhanced photophysical properties, avoid the susceptibility of these chromophores to undergo nucleophilic attack and aggregate formation. This supramolecular insulation was also found to be useful for improving the conducting performance of polymers.[32]

The spatial arrangement of the hydrogen-bonding acceptors of Pechmann dilactams **2** are well oriented to form two bifurcated hydrogen bonds with tetrabenzylamide macrocycles (Fig. 1c).[30,33–42] Thus, they are potential templates for the formation of the corresponding hydrogen-bonded [2]rotaxanes by a clipping procedure. Herein, we report the synthesis of a series of mechanically interlocked aza-Pechmann dyes bearing tetralactams rings. To explore their properties, we have prepared a wide range of such species by varying not only the substituents at the chromophore but also at the isophthalamide moiety of the macrocycle. In this study we evidence that the mechanical bond greatly enhances the thermal stability of the interlocked Pechmann dilactams. Moreover, the structure of the surrounding macrocycle is a molecular design parameter that can be used to non-covalently fine-tune the photophysical and redox properties of the encapsulated dye. The herein disclosed synthesis of mechanically interlocked aza-Pechmann dyes should hopefully pave the way for the construction of unprecedented and groundbreaking novel devices based on this donor–acceptor-donor structures.

Results and discussion

Synthesis and structural characterization of interlocked aza-Pechmann dyes 3a–i

The synthesis of dilactams **2a–d** (Scheme 1) was carried out following previously described methods (Scheme S1†).

We were especially interested in the thiophene-derived dyes (**2b–d**), because thiophene-substituted acceptor molecules are ubiquitous in the structure of organic semiconductors[43] and molecular wires.[32] For comparison, the Pechmann dilactam **2a** with two phenyl substituents at the dye-core was also prepared. Hydrophobic alkyl chains of twelve (**2a** and **2b**), four (**2c**) and two carbon atoms (**2d**), were introduced into the chromophore
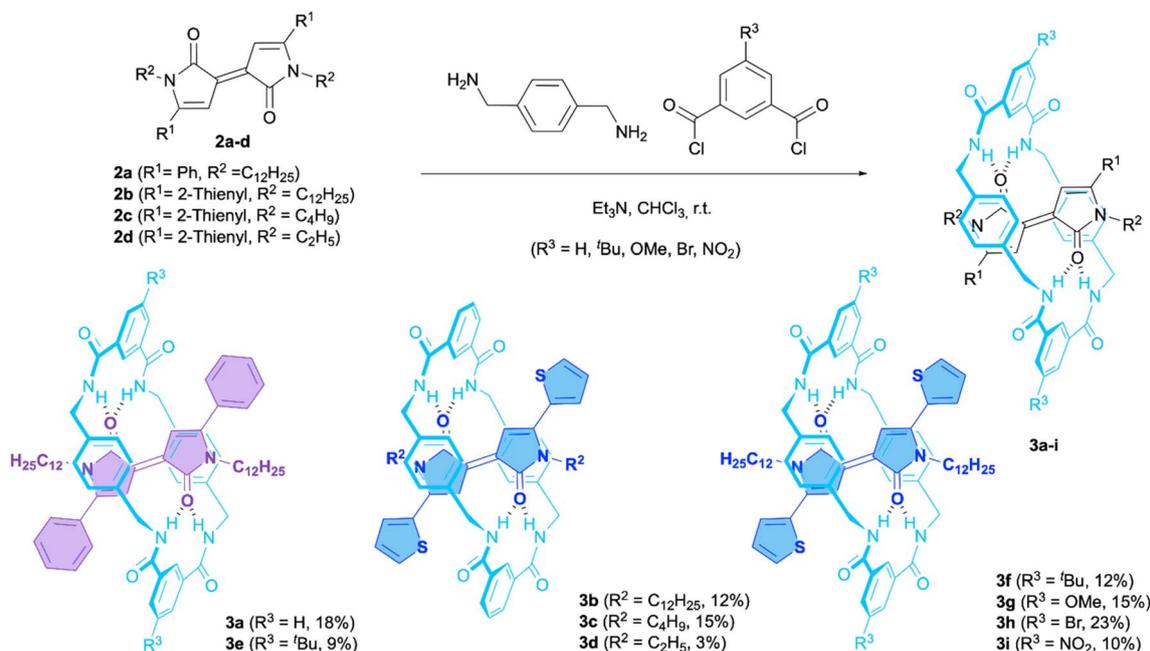
Scheme 1 Synthesis of interlocked Pechmann dilactams **3a–i** from the corresponding free dyes **2a–d**.

skeleton to establish the influence of the steric size at this position on the stability of mechanical bond. [2]Rotaxanes **3a–i** were assembled through a five-component reaction from the Pechmann dilactams **2a–d**, *p*-xylylenediamine and the appropriate diacyl chloride in the presence of Et₃N (Scheme 1).[34] The successful isolation of rotaxanes **3a–c** and **3e–i** in modest yields (9–23%) demonstrates that dilactams **2a–c** can act as reasonably good templates in this type of clipping methodology. However, [2]rotaxane **3d**, with less-steric demand substituents at the nitrogen atoms of the thread, was obtained in very low yield as a mixture with the free axle and other unknown compounds (ESI†). Apparently, the size of R² must be larger than an ethyl group in order to kinetically stabilize the mechanical bond.[44] Chloroform solutions of the interlocked dyes **3** display vivid violet (R¹ = Ph) or blue colours (R¹ = 2-thienyl) (see below). ¹H-NMR spectra of **3a–i** show diagnostic features indicative of their interlocked structure as outlined in Fig. 2a, with **3b** as the model substrate. Thus, the resonances for Hₐ and H_b protons, placed at the dilactam core and the thiophene ring, experience significant upfield shifts (Δδ = −0.82 ppm and −0.76 ppm, respectively) due to the anisotropic shielding effect of the tetrabenzylamide macrocycle. The corresponding ¹H,¹H-NOESY spectrum reveals cross peaks relating Hₐ at the dye component with H_C, H_D and H_F inside the cavity of the macrocycle (Fig. 2b). All the protons involved in intermolecular NOE contacts are separated by less than 4.0 Å in the X-ray structure of **3b** (see below). Finally, the formation of the interlocked structures is also supported by ESI-HRMS spectra where the protonated molecular ions are observed as intense peaks (Fig. 2d and S5–S12†). Curiously, the mass spectra of all free dyes **2a–d** display the presence of peaks corresponding to dimeric and even trimeric species (Fig. 2c and S1–S4†) demonstrating the beneficial effect of the mechanical bond avoiding aggregation.

Additionally structural characterization was gained from single-crystal X-ray diffraction analyses of **3b** and **3c** which reveal a perfect fit between the dyes and the benzylic amide ring in terms of the complementary position of the hydrogen-bonding acceptor and donors (Fig. 3a and b). In both crystal structures, the macrocycles are engaged in bifurcated hydrogen bonds *via* their amide groups with the oxygen atoms at the dye core. However, the thiophene rings are coplanar with the dilactam skeleton in **3b**, dihedral angles of 4–7°, in marked contrast to rotaxane **3c** where the thiophene rings and the dye core intersect at an angle of 38°.

The higher level of conjugation in **3b** is reflected in the shorter bond lengths between the lactam and thiophene rings (1.438 Å) compared with the equivalent length in **3c** (1.452 Å). Nevertheless, we cannot discard that these structural differences are due to packing effects, since resonances of Hₐ in their respective NMR spectra are rather similar (ESI†). Curiously, while in **3b** the thienyl groups are s-*trans* respect to the carbonyl group at the γ-lactams, in **3c** the thienyl groups have an s-*cis* arrangement. The two xylylene walls stack against the dye, being the centroid–centroid distance between the macrocycle's parallel xylylene units very similar in both structures (7.16 Å). The crystal structure of **3b** along the *a* and *b* axes shows the interdigitation of the dodecyl chains (Fig. S16 and S17†). This pattern significantly contributes to the stability of the crystalline packing and is likely responsible for the observed flattening of the macrocycle of **3b**, as opposed to the chair-like conformation seen in the ring of **3c** (see also Fig. S15c and S18c†).

Finally, we carried out NMR diffusion measurements[45–47] on a solution of rotaxane **3c** (2 × 10⁻³ M, CDCl₃, 20 °C) (see ESI† for experimental details) and determined a *D* value of 6.17 × 10⁻¹⁰ m² s⁻¹. The hydrodynamic radius (r_H) of **3c** was calculated from the *D* value by using the Stokes–Einstein equation.[48] The value of r_H (6.1 Å, standard deviation ± 0.1 Å) is in good agreement
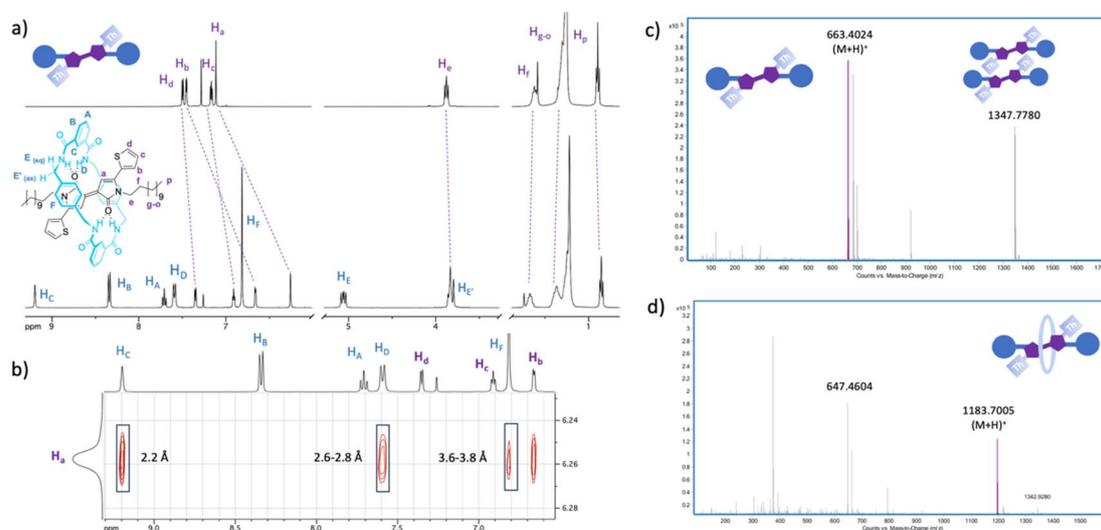

Fig. 2 (a) ¹H NMR spectra (400 MHz, CDCl₃, 25 °C) of the free dye **2b** and the [2]rotaxane **3b**; (b) selected section of the ¹H,¹H-NOESY spectrum (400 MHz, CDCl₃, 25 °C) of **3b** showing cross peaks resulting from contacts between the axle and the macrocycle (distances measured in the X-ray structure of **3b** are also specified); (c) ESI-HMRS spectrum showing peaks for **2b** and the corresponding dimeric aggregate **2b·2b**; (d) ESI-HMRS spectrum of **3b** showing the molecular ion for the rotaxane.
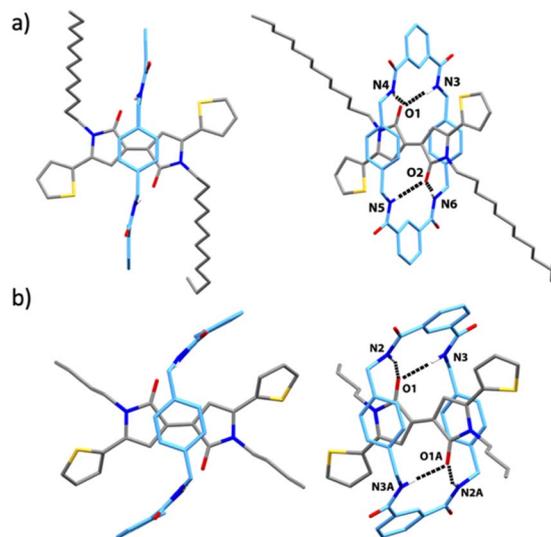
Fig. 3 (a) X-ray structure of **3b** from two different perspectives. Intramolecular HB lengths [Å] (and angles [°]): N3HO1 2.05 (168); N4HO1 2.41 (174); N5HO2 2.15 (172); N6HO2 2.31 (178); (b) X-ray structure of **3c** from two different perspectives. Intramolecular HB lengths [Å] (and angles [°]): N2HO1/N2AHO1A 2.10 (164); N3HO1/N3AHO1A 2.16 (171). For clarity, selected hydrogen atoms are omitted.

with the size (6.1 Å) estimated from the X-ray structure determination.[49]

Study of the rotational motion of the macrocycle in [2]rotaxanes 3a and 3c

The energy barrier for macrocyclic ring rotation around the thread offers a quantification of the strength of the interactions between these two components.[33,34,50] In $C_2D_2Cl_4$ at 25 °C, two sets of signals are observed for the benzylic methylene protons $H_{E/E'}$ of rotaxanes **3a–i**, illustrated for **3b** in Fig. 2a, indicating that the pirouetting of the macrocycle is slow on the NMR time scale.[51] Variable-temperature (VT) ^{1}H NMR experiments show that the exchange is so low in **3c** that is not possible to reach the fast exchange regime below 129 °C (Fig. S19 and S20†). Assuming this value as the corresponding coalescence temperature, the calculated activation energy results in a value of 18.0 ± 0.2 kcal mol⁻¹. Additionally, the rate of the macrocycle rotation in **3a** was estimated by line shape analysis of its ^{1}H NMR spectra at different temperatures (Fig. S21–S23†), which gave an energy barrier at 25 °C of 17.3 kcal mol⁻¹. This value is much higher compared to that of similar [2]rotaxanes bearing fumaramide threads ($\Delta G^{\neq} = 13.4$ kcal mol⁻¹),[50] which have close-to-ideal arrangements of hydrogen-bonded acceptor and donor. In fact, **3a** and **3c** possess ones of the highest energy barriers found for the rotation of [2]rotaxanes built with benzylic amide macrocycles[35,52] as result of the strong intra-component interactions between the dye and the benzylic amide macrocycle joint to the rigidity and bulkiness of the thread. The activation enthalpy and entropy for the pirouetting of the macrocycle in **3a** were derived by Eyring analysis and resulted in values of 16.5 kcal mol⁻¹ and −2.6 cal mol⁻¹ K⁻¹ (Table S6†).

Thermal stability

To test the chemical stabilities of rotaxanes **3** and compare them with those of the free dyes, the progress of the thermolysis of **2b**, **2c** and **3b**, **3c** was simultaneously monitored by ^{1}H NMR spectroscopy (Fig. S24–S30†). Thus, we heated separate samples of each compound in $C_2D_2Cl_4$ at 120 °C in the presence of durene as internal standard. Regarding the thermolysis of **2b**, **2c** we were not able to detect the formation of the corresponding 6,6-*endo*-fused lactams.[8,11,13] Instead, after 3 days we observed that more than 35% of the starting dyes have decomposed into a complex mixture of products from which we were able to identify resonances of two new compounds: *N*-dodecyl-*N*-formylthiophene-2-carboxamide (**4**) and *N*-dodecylthiophene-2-carboxamide (**5**) (Fig. S24†). Both derivatives, **4** and **5**, could be isolated in 13% and 20%, respectively, by conducting the same reaction with **2b** at larger scale (ESI†). The formation of **4** and **5** can be rationalized by the formation of thiophene-2-carboxylic acid through oxidative degradation of **2b**, and further amidation.[1]

By contrast, rotaxanes **3b**, **3c** proved to be much more stable under the same reaction conditions (Fig. S28–S30†). In fact, the ^{1}H NMR spectrum of **3c** showed that approximately 92% of the starting rotaxane was still present in the reaction mixture after 23 days.[53] Surprisingly, we did not observe resonances for the free dyes **2b**, **2c** formed by dethreading of **3b**, **3c**. The reactivity differences between **2b**, **2c** and **3b**, **3c** are attributed to the steric protection provided by the macrocycle and the efficient H-bonding between the two components within the rotaxanes.

Thermal stabilities of **2b**, **2c** and **3b**, **3c** were also examined in the solid state by thermogravimetric analysis (TGA) with analogous results. Thus, TGA experiments reveal that naked dyes **2b**, **2c** decompose above 309–325 °C (Fig. S31 and S32†). By contrast, rotaxanes **3b**, **3c** are thermally stable below 380 °C (Fig. S33 and S34†), which underlines the notable shielding effect of the mechanical bond in these conditions.

Photophysical properties

The UV-vis spectra of interlocked dyes **3a–c** and **3f–i** were recorded in CHCl₃ and compared to those of the Pechmann dilactams **2a–c** (Fig. 4a, S35–S44†). The spectra of the free dyes and the rotaxanes share common broad bands in the visible region along with a second band around 300 nm. However, the presence of phenyl or thienyl substituents at the dilactam core and, especially, the encapsulation of the dye in rotaxanes **3** induces notable changes in the visible region of the spectra. Thus, the UV-vis spectrum of **2a** displays a broad band at $\lambda_{max} = 558$ nm (Fig. 4a and Table 1, entry 1). As a result, solutions of **2a** in CHCl₃ appear violet. The substitution of the two phenyl groups by thienyl groups in the dye-skeleton induces a bathochromic shift of 49 nm for both **2b** and **2c** ($\lambda_{max} = 607$ nm) and, consequently, a change to blue colour (Fig. 4a and Table 1, entries 2 and 3).

Remarkably, the photophysical properties of **2a–c** are altered when the dyes are encapsulated inside the benzylic amide macrocycle. A comparison of the spectra of **2a–c** and **3a–c** ($R^3 =$ H) reveals a notable bathochromic shift of the absorption
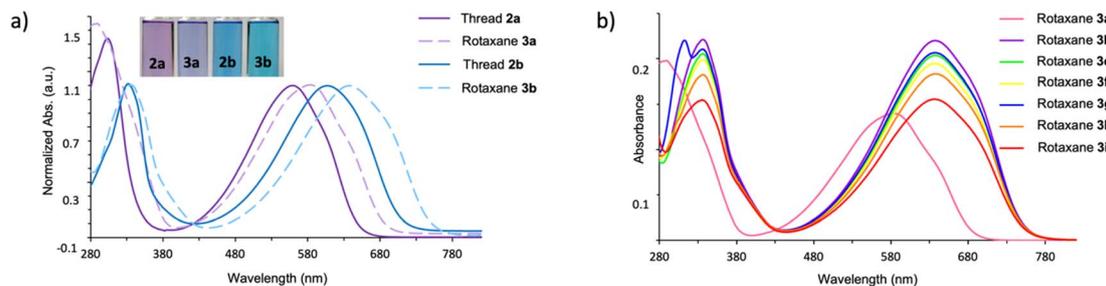
Fig. 4 (a) UV-vis absorption spectra of threads **2a**, **2b** and rotaxanes **3a**, **3b** in CHCl$_3$ ($c \approx 10^{-5}$ M) and photograph of CHCl$_3$ solutions ($c \approx 10^{-5}$ M) of compounds **2a**, **2b** and **3a**, **3b**; (b) UV-vis absorption spectra of rotaxanes **3a–c** and **3f–i** in CHCl$_3$ ($c \approx 10^{-5}$ M).

Table 1 Maxima absorption bands (λ_{max}) in the UV-vis spectra and peak potentials E (V, *vs.* Ag/Ag$^+$) ($E_{pc} = E_{1/2}$) and E_p^{ox} (corresponding to the max. current) in DCM-Bu$_4$NPF$_6$ (0.1 M) as SSE (scan rate: 50 mV s^{-1}) of dyes **2** and rotaxanes **3**

Entry	Compd	λ_{max}	E_{pc1}	E_{pc2}	$E_{onset}^{red1\ a}$	E_p^{ox}	$E_{onset}^{ox\ a}$	Energy HOMO^b/eV	Energy LUMO^b/eV	HOMO–LUMO gap ΔE/eV
1	**2a**	558	—	—	—	—	—	—	—	—
2	**2b**	607	−0.937	−1.374	−0.867	+0.927	+0.724	−5.134	−3.543	1.591
3	**2c**	607	−0.944	−1.387	−0.842	+0.923	+0.684	−5.094	−3.568	1.526
4	**3a**	583	—	—	—	—	—	—	—	—
5	**3b**	638	−0.730	−1.536	−0.653	+1.007	+0.902	−5.312	−3.757	1.555
6	**3c**	637	−0.742	−1.561	−0.648	+1.076	+0.871	−5.281	−3.762	1.519
7	**3f**	637	−0.757	−1.560	−0.667	+1.064	+0.902	−5.312	−3.743	1.569
8	**3g**	638	−0.762	−1.595	−0.671	+1.114	+0.937	−5.347	−3.739	1.608
9	**3h**	638	−0.703	−1.515	−0.612	+1.090	+0.914	−5.324	−3.798	1.526
10	**3i**	637	−0.583	−1.691	−0.511	+1.105	+0.941	−5.351	−3.899	1.452

^{a} E_{onset} is the first onset oxidation or reduction potential measured from CV *vs.* Ag/Ag$^+$. ^{b} Estimated by applying the following equations: LUMO = $-(E_{onset}^{red1} + 4.41)$ eV, HOMO = $-(E_{onset}^{ox} + 4.41)$ eV.[60]

maxima of 25 nm for the interlocked dye **3a** ($\lambda_{max} = 583$ nm) and 31 nm for **3b**, **3c** ($\lambda_{max} = 637$–638 nm) (Fig. 4a and Table 1, entries 4–6).[30,31] The absorption spectra of rotaxanes **3f–i** with substituents of different electronic nature at the macrocycle show an analogous pattern (Fig. 4b and Table 1, entries 7–10).

Finally, we recorded the spectra of **2b** and **3b** in eight solvents of different polarity (Fig. S45–S58†). Negative solvatochromic effects, ascribed to the charge-transfer nature of the electronic transition, have been previously observed for different classes of donor–acceptor molecules.[7,54,55] In our case, we expected to find a different pattern for the free dye **2b** and the rotaxane **3b** especially in polar solvents where the intercomponent hydrogen bonds within the rotaxane are weakened by interaction with the solvent. However, both type of compounds shows analogous slight, blue-shifted absorptions (14 and 10 nm, respectively) on increasing the polarity of the media (Tables S7 and S8†). Clearly, the restricted mobility of the ring in these aza-Pechmann templates precludes a stronger solvatochromic effect as one may expect from a interlocked dye in a polar solvent.[56]

Computational study

We computed the energies of the frontier molecular orbitals (FMOs) and their UV-vis absorption maxima for all the optimized structures of model dye **2j** and model rotaxanes **3j–n** (Fig. 5a).[11] For simplification, the long chains at R^2 of threads **2** and rotaxanes **3** were substituted by methyl groups, and the Br

atoms at **3h** were substituted by Cl atoms at **3m**. The calculations predict that [2]rotaxanes **3j–n** present a pondered average of λ_{max} ranging from 614 to 637 nm (Tables S9 and S10†), corresponding to their HOMO → LUMO transitions, higher than that of the thiophene-containing thread **2j** ($\lambda_{max} = 611$ nm). Thus, the red shift that the dyes experience when surrounded by the macrocycle in rotaxanes **3** is consistent with a narrower HOMO–LUMO gap. This finding aligns with the experimental observations from the electrochemical study (see below). The HOMO and LUMO energies of thread **2j** were calculated to be −5.33 eV and −2.91 eV, respectively (Table S9†). The introduction of the macrocyclic ring around the thread stabilizes both FMOs, with a greater effect observed in rotaxanes substituted by an EWG on the macrocycle, like **3m** (R=Cl, −5.82 and −3.37 eV) and **3n** (R=NO$_2$, −5.90 and −3.43 eV) (for a more complete picture see ESI†). Fig. 5b and c show the FMO of thread **2j** and rotaxane **3j** (Fig. S59† contains the FMOs of all computed rotaxanes). The FMOs of the thread are located mainly at both γ-lactams motifs. Curiously, when the macrocycle is present, these molecular orbitals remain along the molecular backbone of the thread. Thus, the *p*-xylylene fragment of the macrocycle directly interacts with the dye skeleton, which might be responsible for the bathochromic shift of the HOMO–LUMO transitions. It should be noted that both FMOs of all rotaxanes are well distributed over their conjugated backbone benefiting charge carrier transporting.[21]
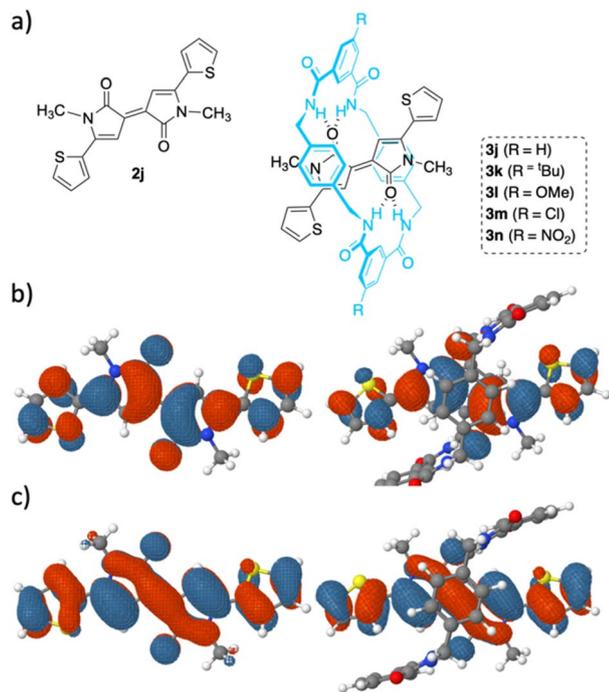
Fig. 5 (a) Structure of the model dye 2j and model [2]rotaxanes 3j–n, which were the subject of the computational study; (b) and (c) contour plots of the frontier molecular orbitals (HOMO and LUMO, respectively) of the thread 2j (left) and rotaxane 3j (right) at the SMD(CHCl$_3$)/M062/DGDZVP level of theory.

Fig. 6 Cyclic voltammetry of 2b (green curves) and 3g (cathodic scan-blue curve and anodic scan-red curve) (both 3×10^{-5} M) in DCM-TBAPF$_6$-50 mV s^{-1}. Pt(−), Pt(+), sat Ag/Ag$^+$ (reference electrode).

The R substituent at the macrocycle is far from the interacting-site, which explains why only slight differences among the spectra of model interlocked dyes 3k–n are expected.

Electrochemical study

The electrochemical properties of dyes 2b, 2c and rotaxanes 3b, 3c, 3f–i were studied by cyclic voltammetry (CV) at 25 °C (Fig. S60–S77†). The peak potentials are summarized in Table 1. Pechmann lactams 2 show two pseudo-reversible reduction peaks (two single heterogeneous electron transfers, Fig. 6 and Table 1, entries 2 and 3), the first one corresponding to the initial formation of a radical anion and the second to a stable dienolate anion (Scheme S2†). However, the anodic scan shows a broad (or a shoulder peak such that observed in 2c, Fig. S62†) non-reversible oxidation peak that corresponds to a two-electron transfer process leading to a thienyl-dication, which could polymerize in the presence of new molecules of non-interlocked dye 2 (Scheme S2†).[57–59]

Compared to the CV of 2b and 2c, the first cathodic potential values in rotaxanes 3b, 3c and 3f–i are shifted to less negative potentials, i.e. easier reduced (better acceptors) (Fig. 6 and Table 1, entries 5–10). This effect reflects the additional stabilization of the first radical anion by hydrogen bonding from the Leigh-type macrocycle. At the same time, the second reduction peak is negatively shifted (Fig. 6 and Table 1, entries 5–10), as expected due to the hindered effect of the macrocycle on the subsequent adsorption of the radical at the cathode surface prior to its discharge leading to a O-centered dianion (dienolate).
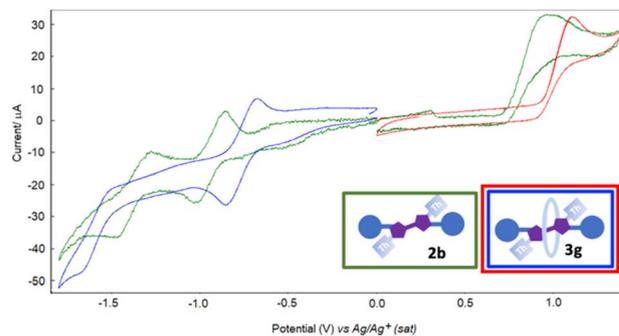
The mechanical bond is also responsible in 3b, 3c and 3f–i for lowering the rate constant of this second heterogeneous electron-transfer at the cathode, that lose some reversibility (Fig. 6).

The anodic peak in rotaxanes 3 still corresponds to a 2e$^-$ process to form a dication, but its potential is shifted to a more positive value compared to the respective naked threads (Fig. 6 and Table 1). This effect of the macrocycle is common to all the studied rotaxanes: anodic shift to more positive potentials, agreeing with higher difficulties to be oxidized, as expected when HOMO energies in rotaxanes are stabilized in comparison with the corresponding threads 2. The dielectronic and still non reversible anodic peak in 3b, 3c and 3f–i shows, however, in some cases slight reversibility (3b) that agrees with an inhibition by the macrocycle of the plausible anodic polymerization (above suggested) in the oxidation of the thread.

In the cathodic scan, electron-withdrawing substituents at the macrocycle (such as Br or NO$_2$) highlight a shift to less negative reduction potential of the first electron-transfer (Table 1, entries 9 and 10). However, electron-donating substituents (such as MeO or ^{t}Bu) are shifted in minor extent (Table 1, entries 7 and 8). This effect can be due to the higher H-bonding strength caused by the EWG substituents. The greater the strength of the hydrogen bonds, the higher is the stabilization of the radical anion, and this is noted in a greater displacement of the first reduction potential.

Overall, the voltametric data provide a complete picture of the energy of the frontier orbitals in interlocked dyes 3 and how they are affected by the presence and nature of the mechanically interlocked macrocycle. First, they indicate that the incorporation of aza-Pechmann dyes as threads in the interlocked molecules 3 stabilizes both HOMO (from −0.18 to −0.22 eV) and LUMO (from −0.20 to −0.36 eV). As a result, the HOMO–LUMO gap energy of rotaxanes 3b, 3c and 3f–i experiences a decrease in all cases, in agreement with that we found in the UV-vis data. Moreover, there are subtle differences depending on the substituent at the macrocycle. Thus, the HOMO–LUMO gap energies experience drops up to −0.07 eV for 3h (R^3=Br) and −0.14 eV for 3i (R^3=NO$_2$) in full agreement with the computational study.

Conclusions

We have described the first synthesis of mechanically interlocked aza-Pechmann dyes. In this family of rotaxanes with benzylic amide macrocycles, the double γ-lactam core perfectly performs as template, the oxygen atoms of the dye driving the clipping reaction of the macrocycle by hydrogen-bonding interactions, as evidenced by NMR and single-crystal X-ray diffraction.

The high energy barrier for macrocyclic ring rotation around the dyes offers a quantification of the high strength of the interactions with the macrocycle. Moreover, the thermal stabilities of the rotaxanes are much higher than those of the free dyes in both solution and the solid state, illustrating the stabilizing effect of the macrocycle. In addition, absorption, and electrochemical measurements evidence that the macrocycle can modulate the optoelectronic and redox properties of the aza-Pechmann dyes. Thus, computational and electrochemical studies demonstrate that the presence of the benzylic amide macrocycle stabilizes the HOMO and LUMO frontier orbitals of the free dyes when converted into rotaxanes. Furthermore, the electrochemical study shows that the HOMO/LUMO levels can be slightly modulated by the electronic nature of substituents at the macrocycle.

Overall, this work makes available a method to prepare mechanically interlocked nitrogenated Pechmann dyes and provides a proof-of-concept of the effects that the interlocked macrocycle can have on their properties, opening the door to new families of synthetic materials than combine the properties of aza-Pechmann dyes with the dynamic properties of rotaxanes. The advent of groundbreaking technologies in cutting-edge sectors such as biomedicine, materials science, and nanotechnology are stimulating an increasing demand for dyes that offer superior performance features. The integration of aza-Pechmann skeletons as axles in rotaxanes could attract the interest of researchers working in the colorant field, opening avenues for future enticing applications. By deepening our grasp of the interplay between structure and activity, future investigations could precisely adjust the molecular attributes of these intriguing substances, thereby maximizing their practical effectiveness.

Author contributions

The manuscript was written through contributions of all authors. All authors have given approval to the final version of the manuscript.

Conflicts of interest

There are no conflicts to declare.

Data availability

Synthesis and experimental data of compounds **2** and **3**, ESI-HRMS spectra of all new compounds, crystal data and structure refinement for **3b** and **3c**, determination of the constant rates and activation parameters for the pirouetting of the macrocycle in **3a** and **3c**, thermolysis study of **2b**, **2c** and **3b**, **3c**, TGA experiments of **2b**, **2c** and **3a–c**, UV-vis spectra of **2** and **3**, computational study and electrochemical analysis of **2** and **3**, and NMR spectra of all new synthesized compounds are given in the ESI† for this manuscript.

Acknowledgements

Notes and references

1 E. Klingsberg, The Chemistry of the Pechmann Dyes, *Chem. Rev.*, 1954, **54**, 59–77.

2 M. T. Bogert and J. J. Ritter, The Constitution of the So-Called "Pechmann Dyes" and the Mechanism of Their Formation from Beta-Benzoylacrylic Acid, *Proc. Natl. Acad. Sci. U. S. A.*, 1924, **10**, 363–367.

3 J. Silver, M. T. Ahmet, K. Bowden, J. R. Miller, S. Rahmat, C. A. Reynolds, A. Bashall, M. McPartlin and J. Trotter, Electrochromic Behaviour and X-Ray Structure Analysis of a Pechmann Dye, (E)-5,5′-Diphenyl-3,3′-bifuranylidene-2,2′-dione, *J. Mater. Chem.*, 1994, **4**, 1201–1204.

4 K. Bowden, R. Etemadi and R. J. Ranson, Reactions of Carbonyl Compounds in Basic Solutions. Part 17. The Alkaline Hydrolysis of Substituted (E)-5,5′-Diphenylbifuranylidenediones and 3,7-Diphenylpyrano[4,3-c]pyran-1,5-diones, *J. Chem. Soc., Perkin Trans. 2*, 1991, 743–746.

5 K. Bowden, W. M. F. Fabian and G. Kollenz, Semi-empirical AM1 and PM3 Molecular Orbital Calculations on the Mechanism of the Hydrolysis of Unsaturated Lactones: Substituted (E)-5,5′-Diphenylbifuranylidenediones and 3,7-Diphenylpyrano[4,3-c]pyran-1,5-diones, *J. Chem. Soc., Perkin Trans. 2*, 1997, 547–552.

6 A. Efrem, M. Courté, K. Wang, D. Fichou and M. Wang, Synthesis and Characterization of γ-Lactone-Pechmann Dye Based Donor-acceptor Conjugated Polymers, *Dyes Pigm.*, 2016, **134**, 171–177.

7 A. Dessi, M. Bartolini, M. Calamante, L. Zani, A. Mordini and G. Reginato, Extending the Conjugation of Pechmann Lactone Thienyl Derivatives: A New Class of Small Molecules for Organic Electronics Application, *Synthesis*, 2018, **50**, 1284–1292.

8 H. Irikawa, N. Adachi and H. Muraoka, Preparation and Absorption Spectral Properties of the Nitrogen Analogs of a Pechmann Dye and Its Isomeric Pyrano[4,3-c]pyran-1,5-dione, *Heterocycles*, 1998, **48**, 1415–1422.

9 T. Aysha, M. El-Sedik, H. M. Mashaly, M. A. El-Apasery, O. Machalický and R. Hrdina, Synthesis, Characterisation, and Applications of Isoindigo/Pechmann Dye

Heteroanalogue Hybrid Dyes on Polyester Fabric, *Color. Technol.*, 2015, **131**, 333–341.

10 A. G. Newsome, C. A. Culver and R. B. van Breemen, Nature's Palette: The Search for Natural Blue Colorants, *J. Agric. Food Chem.*, 2014, **62**, 6498–6511.

11 E. A. B. Kantchev, T. B. Norsten, M. L. Y. Tan, J. J. Y. Ng and M. B. Sullivan, Thiophene-Containing Pechmann Dyes and Related Compounds: Synthesis, and Experimental and DFT Characterisation, *Chem.–Eur. J.*, 2012, **18**, 695–708.

12 T. Aysha, S. Luňák, A. Lyčka, J. Vyňuchal, Z. Eliáš, A. Růžička, Z. Padělková and R. Hrdina, Synthesis, Structure, Absorption and Fluorescence of Pechmann Dye Heteroanalogues, *Dyes Pigm.*, 2013, **98**, 530–539.

13 A. Dessi, A. Sinicropi, S. Mohammadpourasl, R. Basosi, M. Taddei, F. Fabrizi de Biani, M. Calamante, L. Zani, A. Mordini, P. Bracq, D. Franchi and G. Reginato, New Blue Donor–Acceptor Pechmann Dyes: Synthesis, Spectroscopic, Electrochemical, and Computational Studies, *ACS Omega*, 2019, **4**, 7614–7627.

14 L. Bhattacharya, G. Gogoi, S. Sharma, A. Brown and S. Sahu, Promising Small Molecule Pechmann Dye Analogue Donors with Low Interfacial Charge Recombination for Photovoltaic Application: A DFT Study, *Mater. Today Commun.*, 2021, **28**, 102555.

15 Z. Cai, Y. Guo, S. Yang, Q. Peng, H. Luo, Z. Liu, G. Zhang, Y. Liu and D. Zhang, New Donor–Acceptor–Donor Molecules with Pechmann Dye as the Core Moiety for Solution-Processed Good-Performance Organic Field-Effect Transistors, *Chem. Mater.*, 2013, **25**, 471–478.

16 K. C. Lee, H. R. Lee, S.-H. Kang, J. Lee, Y. I. L. Park, S. M. Noh, J. H. Oh and C. Yang, An Efficient Lactone-to-Lactam Conversion for the Synthesis of Thiophene Pechmann Lactam and the Characterization of Polymers Thereof, *Polym. Chem.*, 2018, **9**, 5234–5241.

17 Z. Cai, Z. Liu, H. Luo, P. Qi, G. Zhang and D. Zhang, π-Extented Conjugated Polymers Entailing Pechmann Dye Moieties for Solution-Processed Ambipolar Organic Semiconductors, *Chin. J. Chem.*, 2014, **32**, 788–796.

18 Z. Cai, H. Luo, P. Qi, J. Wang, G. Zhang, Z. Liu and D. Zhang, Alternating Conjugated Electron Donor–Acceptor Polymers Entailing Pechmann Dye Framework as the Electron Acceptor Moieties for High Performance Organic Semiconductors with Tunable Characteristics, *Macromolecules*, 2014, **47**, 2899–2906.

19 S.-F. Yang, Z.-T. Liu, Z.-X. Cai, H.-W. Luo, P.-L. Qi, G.-X. Zhang and D.-Q. Zhang, Conjugated Donor–Acceptor Polymers Entailing Pechmann Dye-Derived Acceptor with Siloxane-Terminated Side Chains Exhibiting Balanced Ambipolar Semiconducting Behavior, *Macromolecules*, 2016, **49**, 5857–5865.

20 H. Luo, X. Dong, Z. Cai, L. Wang and Z. Liu, Pechmann Dye-Based Molecules Containing Fluorobenzene Moieties for Ambipolar Organic Semiconductors, *Asian J. Org. Chem.*, 2018, **7**, 592–597.

21 P. Qi, Z. Wang, Z. Liu, S. Yang, Y. Yang, J. Yao, G. Zhang and D. Zhang, Conjugated Donor–Acceptor Terpolymers Entailing the Pechmann Dye and Dithienyl-

Diketopyrrolopyrrole as co-Electron Acceptors: Tuning HOMO/LUMO Energies and Photovoltaic Performances, *Polym. Chem.*, 2016, **7**, 3838–3847.

22 E. Arunkumar, C. C. Forbes and B. D. Smith, Improving the Properties of Organic Dyes by Molecular Encapsulation, *Eur. J. Org Chem.*, 2005, 4051–4059.

23 J. J. Gassensmith, E. Arunkumar and B. D. Smith, in *Molecular Encapsulation*, 2010, pp. 309–325.

24 Y. Ohishi, K. Nishioki, Y. Miyaoka, K. Serizawa, S. Sugawara, K. Hayashi, D. Inoue, M. Iwamura, S. Yokoyama, J. Chiba and M. Inouye, A Versatile Synthetic Method for Photophysically and Chemically Stable [5]Rotaxane-Type Fluorescence Dyes of Various Colors by Using a Cooperative Capture Strategy, *Adv. Opt. Mater.*, 2024, **12**, 2301457.

25 A. Riaño, M. Carini, M. Melle-Franco and A. Mateo-Alonso, Mechanically Interlocked Nitrogenated Nanographenes, *J. Am. Chem. Soc.*, 2020, **142**, 20481–20488.

26 P. Rajamalli, F. Rizzi, W. Li, M. A. Jinks, A. K. Gupta, B. A. Laidlaw, I. D. W. Samuel, T. J. Penfold, S. M. Goldup and E. Zysman-Colman, Using the Mechanical Bond to Tune the Performance of a Thermally Activated Delayed Fluorescence Emitter, *Angew. Chem., Int. Ed.*, 2021, **60**, 12066–12073.

27 L. Andreoni, F. Cester Bonati, J. Groppi, D. Balestri, G. Cera, A. Credi, A. Secchi and S. Silvi, Selective Enhancement of Organic Dye Properties through Encapsulation in Rotaxane Orientational Isomers, *Chem. Commun.*, 2023, **59**, 4970–4973.

28 H. V. Miyagishi, H. Masai and J. Terao, Linked Rotaxane Structure Restricts Local Molecular Motions in Solution to Enhance Fluorescence Properties of Tetraphenylethylene, *Chem.–Eur. J.*, 2022, **28**, e202103175.

29 J. J. Gassensmith, J. M. Baumes and B. D. Smith, Discovery and Early Development of Squaraine Rotaxanes, *Chem. Commun.*, 2009, 6329–6338.

30 E. Arunkumar, C. C. Forbes, B. C. Noll and B. D. Smith, Squaraine-Derived Rotaxanes: Sterically Protected Fluorescent Near-IR Dyes, *J. Am. Chem. Soc.*, 2005, **127**, 3288–3289.

31 J. J. Gassensmith, E. Arunkumar, L. Barr, J. M. Baumes, K. M. DiVittorio, J. R. Johnson, B. C. Noll and B. D. Smith, Self-Assembly of Fluorescent Inclusion Complexes in Competitive Media Including the Interior of Living Cells, *J. Am. Chem. Soc.*, 2007, **129**, 15054–15059.

32 M. J. Frampton and H. L. Anderson, Insulated Molecular Wires, *Angew. Chem., Int. Ed.*, 2007, **46**, 1028–1064.

33 D. A. Leigh, A. Murphy, J. P. Smart and M. Z. Slawin, Glycylglycine Rotaxanes-The Hydrogen Bond Directed Assembly of Synthetic Peptide Rotaxanes, *Angew Chem. Int. Ed. Engl.*, 1997, **36**, 728–732.

34 F. G. Gatti, D. A. Leigh, S. A. Nepogodiev, A. M. Z. Slawin, S. J. Teat and J. K. Y. Wong, Stiff, Sticky in the Right Places: the Dramatic Influence of Preorganizing Guest Binding Sites on the Hydrogen Bond-Directed Assembly of Rotaxanes, *J. Am. Chem. Soc.*, 2001, **123**, 5983–5989.

35 D. M. D'Souza, D. A. Leigh, L. Mottier, K. M. Mullen, F. Paolucci, S. J. Teat and S. Zhang, Nitrone [2]Rotaxanes: Simultaneous Chemical Protection and Electrochemical Activation of a Functional Group, *J. Am. Chem. Soc.*, 2010, **132**, 9465–9470.

36 J. Berna, M. Alajarin and R.-A. Orenes, Azodicarboxamides as Template Binding Motifs for the Building of Hydrogen-Bonded Molecular Shuttles, *J. Am. Chem. Soc.*, 2010, **132**, 10741–10747.

37 R. Ahmed, A. Altieri, D. M. D'Souza, D. A. Leigh, K. M. Mullen, M. Papmeyer, A. M. Z. Slawin, J. K. Y. Wong and J. D. Woollins, Phosphorus-Based Functional Groups as Hydrogen Bonding Templates for Rotaxane Formation, *J. Am. Chem. Soc.*, 2011, **133**, 12304–12310.

38 A. Altieri, V. Aucagne, R. Carrillo, G. J. Clarkson, D. M. D'Souza, J. A. Dunnet, D. A. Leigh and K. M. Mullen, Sulfur-Containing Amide-based [2]Rotaxanes and Molecular Shuttles, *Chem. Sci.*, 2011, **2**, 1922–1928.

39 A. Martinez-Cuezva, A. Pastor, G. Cioncoloni, R.-A. Orenes, M. Alajarin, M. D. Symes and J. Berna, Versatile Control of the Submolecular Motion of Di(acylamino)pyridine-Based [2]Rotaxanes, *Chem. Sci.*, 2015, **6**, 3087–3094.

40 A. Martinez-Cuezva, A. Saura-Sanmartin, T. Nicolas-Garcia, C. Navarro, R.-A. Orenes, M. Alajarin and J. Berna, Photoswitchable Interlocked Thiodiglycolamide as a Cocatalyst of a Chalcogeno-Baylis-Hillman Reaction, *Chem. Sci.*, 2017, **8**, 3775–3780.

41 D. A. Leigh, V. Marcos, T. Nalbantoglu, I. J. Vitorica-Yrezabal, F. T. Yasar and X. Zhu, Pyridyl-Acyl Hydrazone Rotaxanes and Molecular Shuttles, *J. Am. Chem. Soc.*, 2017, **139**, 7104–7109.

42 J. de Maria Perez, M. Alajarin, A. Martinez-Cuezva and J. Berna, Reactivity of Glutaconamides Within [2]Rotaxanes: Mechanical Bond Controlled Chemoselective Synthesis of Highly Reactive α-Ketoamides and their Light-Triggered Cyclization, *Angew. Chem., Int. Ed.*, 2023, **62**, e202302681.

43 H. Dong, C. Wang and W. Hu, High Performance Organic Semiconductors for Field-Effect Transistors, *Chem. Commun.*, 2010, **46**, 5211–5222.

44 A. Martinez-Cuezva, L. V. Rodrigues, C. Navarro, F. Carro-Guillen, L. Buriol, C. P. Frizzo, M. A. P. Martins, M. Alajarin and J. Berna, Dethreading of Tetraalkylsuccinamide-Based [2]rotaxanes for Preparing Benzylic Amide Macrocycles, *J. Org. Chem.*, 2015, **80**, 10049–10059.

45 E. O. Stejskal and J. E. Tanner, Spin Diffusion Measurements: Spin Echoes in the Presence of a Time-Dependent Field Gradient, *J. Chem. Phys.*, 1965, **42**, 288–292.

46 A. Pastor and E. Martinez-Viviente, NMR Spectroscopy in Coordination Supramolecular Chemistry: A Unique and Powerful Methodology, *Coord. Chem. Rev.*, 2008, **252**, 2314–2345.

47 A. Macchioni, G. Ciancaleoni, C. Zuccaccia and D. Zuccaccia, Determining Accurate Molecular Sizes in Solution Through NMR Diffusion Spectroscopy, *Chem. Soc. Rev.*, 2008, **37**, 479–489.

48 The Stokes–Einstein equation: $D = (k_B T)/(6\pi\eta rH)$, where D = diffusion coefficient, k_B = Boltzman constant, T = temperature in degrees Kelvin, η = viscosity of the solvent, and rH = hydrodynamic radius (the radius of a hypothetical sphere that diffuses with the same speed as the particle under examination). See: J. T. Edward, *J. Chem. Educ.*, 1970, **47**, 261–270.

49 The rVDW was determined from the .cif file of **3c**, obtained by X-ray diffraction, by using the program Spartan'24.

50 F. G. Gatti, S. León, J. K. Y. Wong, G. Bottari, A. Altieri, M. A. Farran Morales, S. J. Teat, C. Frochot, D. A. Leigh, A. M. Brouver and F. Zerbetto, Photoisomerization of a Rotaxane Hydrogen Bonding Template: Light-Induced Acceleration of a Large Amplitude Rotational Motion, *Proc. Natl. Acad. Sci. U. S. A.*, 2003, **100**, 10–14.

51 This pirouetting motion corresponds to the 180° rotation of the macrocycle around the thread accompanied by an intracomponent chair-chair flip of the macrocycle.

52 N. Fu, J. J. Gassensmith and B. D. Smith, A New Class of Hydroxy-Substituted Squaraine Rotaxane, *Aust. J. Chem.*, 2010, **63**, 792–796.

53 Due to the presence of a complex mixture of products the amount of free dyes and rotaxanes could not be accurately quantified.

54 A. Baheti, P. Singh, C.-P. Lee, K. R. J. Thomas and K.-C. Ho, 2,7-Diaminofluorene-Based Organic Dyes for Dye-Sensitized Solar Cells: Effect of Auxiliary Donor on Optical and Electrochemical Properties, *J. Org. Chem.*, 2011, **76**, 4910–4920.

55 A. V. Kulinich, E. K. Mikitenko and A. A. Ishchenko, Scope of Negative Solvatochromism and Solvatofluorochromism of Merocyanines, *Phys. Chem. Chem. Phys.*, 2016, **18**, 3444–3453.

56 D. A. Leigh, M. Á. F. Morales, E. M. Pérez, J. K. Y. Wong, C. G. Saiz, A. M. Z. Slawin, A. J. Carmichael, D. M. Haddleton, A. M. Brouwer, W. J. Buma, G. W. H. Wurpel, S. León and F. Zerbetto, Patterning through Controlled Submolecular Motion: Rotaxane-Based Switches and Logic Gates that Function in Solution and Polymer Films, *Angew. Chem., Int. Ed.*, 2005, **44**, 3062–3067.

57 M. Chahma, D. J. T. Myles and R. G. Hicks, Synthesis and Electropolymerization Behavior of Bis (Oligothienyl) Sulfides. Generation of Heteroaromatic Poly(p-phenylene sulfide) Analogs, *Chem. Mater.*, 2005, **17**, 2672–2678.

58 J. E. Dick, A. Poirel, R. Ziessel and A. J. Bard, Electrochemistry, Electrogenerated Chemiluminescence, and Electropolymerization of Oligothienyl-BODIPY Derivatives, *Electrochim. Acta*, 2015, **178**, 234–239.

59 V. M. Suresh and U. Scherf, Electrochemically Generated Conjugated Microporous Polymer Network Thin Films for Chemical Sensor Applications, *Macromol. Chem. Phys.*, 2018, **219**, 1800207.

60 L. Dou, J. Gao, E. Richard, J. You, C.-C. Chen, K. C. Cha, Y. He, G. Li and Y. Yang, Systematic Investigation of Benzodithiophene- and Diketopyrrolopyrrole-Based Low-Bandgap Polymers Designed for Single Junction and Tandem Polymer Solar Cells, *J. Am. Chem. Soc.*, 2012, **134**, 10071–10079.